

Lattice-mismatched and twisted multi-layered materials for efficient solar cells

Efstratios Manousakis

Department of Physics, Florida State University, Tallahassee, FL 32306-4350, USA

(Dated: October 31, 2024)

We argue that alternating-layer structures of lattice mismatched or misaligned (twisted) atomically-thin layers should be expected to be more efficient absorbers of the broad-spectrum of solar radiation than the bulk material of each individual layer. In such mismatched layer-structures the conduction and valence bands of the bulk material, split into multiple minibands separated by minigaps confined to a small-size emerging Brillouin zone due to band-folding. We extended the Shockley-Queisser approach to calculate the photovoltaic efficiency for a band split into minibands of bandwidth ΔE and mini-gaps δG to model the case when such structures are used as solar cells. We find a significant efficiency enhancement due to impact ionization processes, especially in the limit of small but non-zero δG , and a dramatic increase when fully concentrated sun-light is used.

I. INTRODUCTION

Conversion of the energy of solar radiation into electrical form by means of the photovoltaic (PV) effect is widely used in most regions of our planet wasting approximately 80% of it into heat. A key reason for this low efficiency[1] is that the photon energy, from the broad solar radiation-spectrum, absorbed by a single electron-hole pair with energy above the semiconductor band-gap is lost by means into heat. The main mechanisms of this loss is electron-phonon scattering and phonon-emission through which electrons and holes relax to the conduction band-minimum (CBM) or valence-band maximum (VBM). If instead, semiconductors with a relatively large band-gap are chosen in order to avoid the above issue, most of the energy spectrum of the solar radiation is cut off and travels through the material without absorption.

There is a growing effort to fabricate structures with higher PV efficiency. The so-called multi-junction (MJ) solar-cells have reached efficiency at 40% levels. The MJ or tandem solar cell[2] is made by combining a stack of cascaded multiple pn-junctions with various band gaps in order to catch a larger photon energy spectrum. It is an expensive approach and these cells are preferred in space applications.

Various ideas to increase efficiency have been proposed[3], such as, using the role of the interaction of localized electronic states with the conduction band[4, 5]. Highly gap-mismatched alloys[6], where a class of materials forms through alloying of distinctly different semiconductors, have been shown to yield an increased PV efficiency. In addition, the family of the so-called intermediate band solar cells[7], which is based on the idea of forming an impurity band in the semiconductor band gap, could lead to an increased efficiency[8].

Other structures, such as nanotubes, quantum dots, and two-dimensional (2D) halide perovskites have been considered as candidates for solar cells[9] with higher PV efficiency because of multi-carrier generation (MCG)[10–12]. Recently, the impact ionization process, which leads to MCG, was proposed to be effective in strongly correlated insulators[13–15]. More recently, it has been proposed[16, 17] that utilizing Berry curvature dipoles

can lead to optical gain.

It is well-known that films of multilayer structures can be grown by various techniques, including molecular beam epitaxy, chemical vapor deposition or transport or by a more recent technique where entire atomically-thin layers of a crystalline material can be placed on top of another layer. Our discussion will be focused on structures *ABAB...* of alternating atomically-thin of lattice mismatched layers *A* and *B* or of misaligned layers *A* and *B* twisted by opposite angles. Multiple recent reports of successfully realizing twisted layers of materials[18–23] indicate that fabrication of such multilayers of our choice may not be a too-far-in-the-future project. In both of these different situations, a periodic structure with an emerging wavelength significantly larger than the Wigner-Seitz unit cell of each of the layers, can emerge. The electronic band-structure of such structures lives in a Brillouin zone (BZ) which is the result of folding the BZ of each of the individual layers multiple times. Here, we will demonstrate that such a band-structure has characteristic properties that can be tuned to become more efficient absorbers of the solar radiation spectrum.

A multilayer of twisted or lattice-mismatched layers can be used to split a band into minibands which can be used to increase the photo-voltaic (PV) efficiency. The photoexcited electron-hole pair can decay by means of multi-phonon emission to the bottom of the miniband to which it was excited. However, since the bandwidth of each miniband is very small, the energy converted to heat will only be of the order of the bandwidth of each miniband, from where it can only decay by means of recombination or impact ionization. Namely, since there are no states in these multiple mini-gaps, the photoexcited electrons or holes, after they reach the bottom of the particular mini-band, have only two possible decay mechanisms: impact ionization, i.e., by exciting other electron-hole pairs (which leads to carrier multiplication) or by means of electron-hole recombination. Therefore, these materials, have significantly limited the phonon-emission mechanism and, therefore, as we demonstrate here, should be expected to perform more efficiently as absorbers of a larger part of the solar spectrum.

Splitting the bands with small gaps allows those pho-

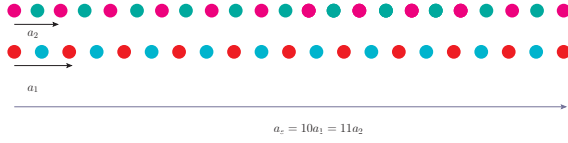


FIG. 1. A ladder formed by two chains having a slight lattice mismatch.

tons with energy inside these gaps to go through the material without been absorbed. However, as we will show, the fraction of the gaped energy interval to that in which there is band presence is small. The presence of such mini-gaps prevents or delays the decay of the electron or hole carrier to the bottom of the original band present in the bulk material before splitting. Furthermore, the band folding generates complex conservation and selection rules for a decay process through phonon emission, which only results in a significant increase of the decay time-scale. This fosters a convenient environment for the impact ionization processes to occur, which lead to carrier multiplication[13–15].

The paper is organized as follows. In the following section we use tight-binding models to illustrate how large bands of bulk semiconductors can split into many mini-bands separated by mini-gaps because of the multi-folding of the Brillouin zone as a result of superlattice formation due to either lattice-mismatch or twisting of atomically thin layers. In Sec. III A we discuss the effects of interactions on these mini-bands. In Sec. III B we discuss the role of the various interaction and decay processes on the relaxation of the photo-excited electron-hole pairs. In Sec. IV we extend the calculation of Shockley and Queisser[1], which was done for a single band, to calculate the photo-voltaic efficiency enhancement when the semiconductor band is split into many bands (all of which are within the energy domain of the solar radiation) of small bandwidth separated by small gaps. Lastly, in Sec. V we discuss our findings and give our concluding remarks.

II. MINIBANDS FROM LARGE BAND-FOLDING

A. A ladder of mismatched chains

As our first example, we use a simple one dimensional (1D) structure to illustrate the effect of lattice mismatch on the electronic band-structure. Two infinite 1D chains are coupled to form the ladder shown in Fig. 1. Each chain consists of two different atoms (a and b) drawn as blue and red for chain 1 (bottom) and magenta and green for chain 2 (top). The unit-cell sizes $a_{1,2}$ for each layer are somewhat different, such that $(M + 1)a_2 = Ma_1$; we have chosen $M = 10$, in such a way that there is the superperiodic lattice with period $a_s = 10a_1 = 11a_2$.

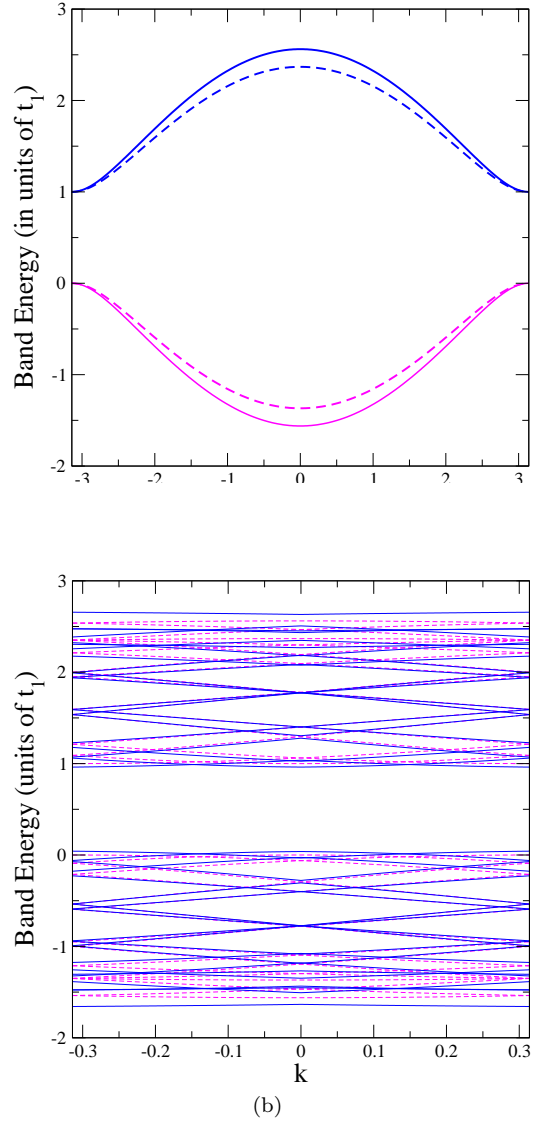


FIG. 2. (a) The bands of each chain separately. The solid (dashed) lines correspond to layer 1 (layer 2) and are plotted versus k_1a_1 (k_2a_2). (b) The band structure of the combined interacting chains.

Namely, the ladder shown in Fig. 1 with 10 unit cells in chain-1 and 11 unit cells in chain-2 repeats itself as the end of the 10th unit-cell of chain-1 lines up with that of end of the 11th unit cell of chain-2. Therefore, the ladder is characterized by a superperiodic structure, with 20 atomic states in chain 1 and 22 atomic states in chain 2. Each chain is described by a simple tight-binding model with different on-site energies $e_{1,2}^{(a)}$ and $e_{1,2}^{(b)}$ for the a and b atoms and with a single hopping integral $t_{1,2}$ from atom a to atom b within each chain 1 and 2, which yields the band-structures:

$$e_{\mu}^{\pm}(k) = \frac{e_{\mu}^{(a)} + e_{\mu}^{(b)}}{2} \pm \sqrt{\left(\frac{e_{\mu}^{(a)} - e_{\mu}^{(b)}}{2}\right)^2 + 4t_{\mu}^2 \cos^2\left(\frac{k_{\mu}a_{\mu}}{2}\right)}, (1)$$

where $\mu = 1, 2$. These band-structures are illustrated in Fig. 2(b) for $t_2/t_1 = 0.9$ and $e_{1,2}^{(a)}/t_1 = 1$ and $e_{1,2}^{(b)} = 0$. The band structure of a non-interacting such ladder is shown by the dotted magenta lines in Fig. 2(b), which consists of 42 minibands obtained by folding the original bands (Fig. 2(a)) into an M -fold smaller BZ (notice the scale of the k axis in Fig. 2(b) as compared to that of the bands in Fig 2(a)). We have introduced constant interaction matrix elements of strength $\delta/t = 0.1$ between adjacent bands to obtain the bands-structure shown by the blue lines in Fig. 2(b). Such interaction can lift the degeneracy between bands at the smaller-BZ corners creating small gaps. If we allow atomic relaxation, these gaps are expected to become somewhat wider.

In summary, by having a lattice mismatch between the two 1D layers, we obtained a folded BZ with a number of bands equal to the number of atomic states in the super-unit-cell obtained as a result of the lattice mismatch. The band-structure can have a main gap of similar size as each isolated chain, while the conduction and valence bands of the coupled chains are split into many mini-bands with mini-gaps. These characteristics are independent of dimension as demonstrated in two 2D examples, next.

B. Mismatched bi-layers

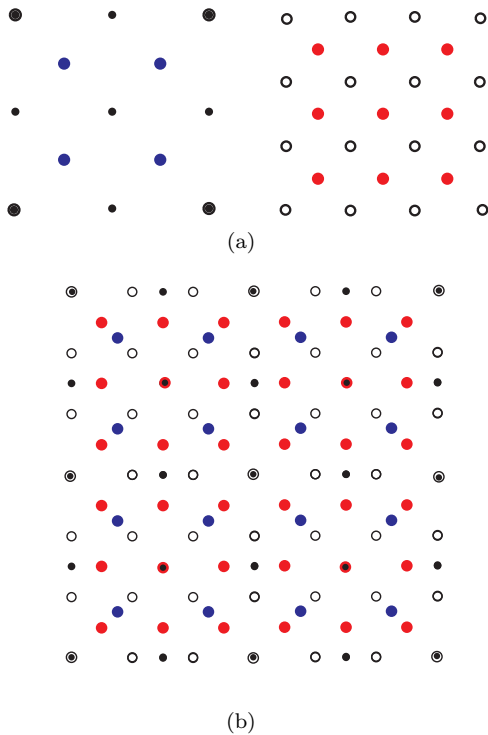


FIG. 3. (a) The top two lattices which when super-imposed give rise to the unit-cell shown at the bottom (b).

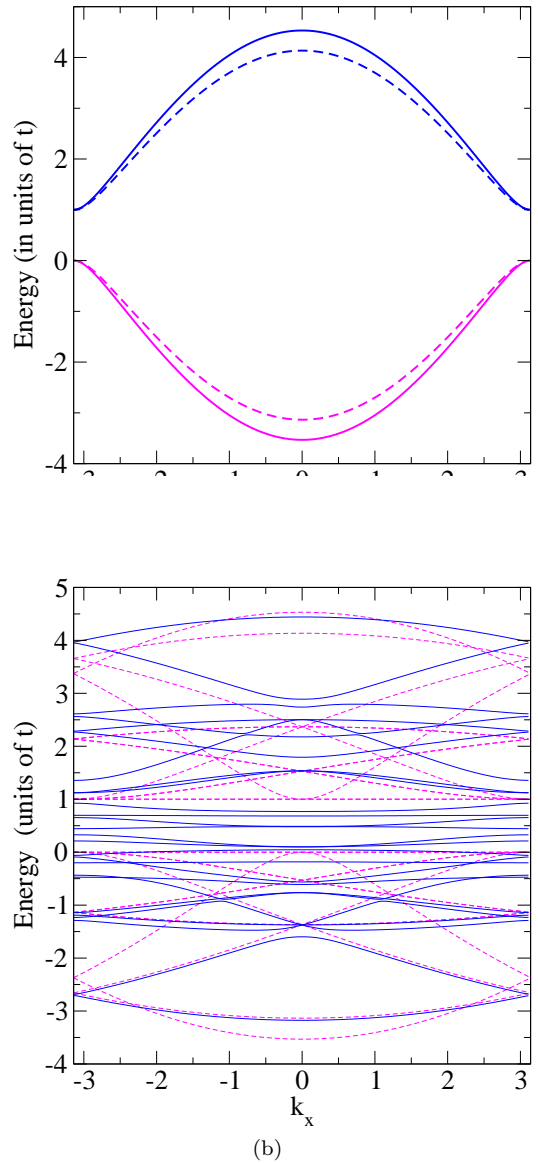


FIG. 4. (a) Bands of the two layers before they are placed on top of each other. (b) The band-structure of the two mismatched layers along the k_x direction.

As a 2D example of lattice-mismatched layers, we consider a square lattice of atoms a and a different atom b at the center of every square. (see Fig. 3(a) left). A second layer of the same structure (Fig. 3(a) right) with the same on-site energies as the first layer, i.e., $e_1^{(a)} = e_2^{(a)} = 1$ and $e_1^{(b)} = e_2^{(b)} = 0$ and just a single hopping $t_{1,2}$ between the atoms a and b of each layer 1 or 2. Then, the two layers are superimposed to form the periodic super-structure shown in Fig. 3(b). As in the one dimensional case in general we can consider the case where $(M+1)a^{(2)} = Ma^{(1)}$ where M can be a large integer. In the example of Fig. 3, a square of 4 unit cells (2×2) of the layer-1 fits exactly a 3×3 square of layer-2.

In this case the corresponding lattice mismatch is very large, i.e., the smaller unit cell $a^{(2)}$ is $3/4$ of the larger unit cell $a^{(1)}$. Without loss of generality, we have considered a rather large mismatch, which would give a rather small supercell in order to make its tight-binding treatment discussed here when we introduce interlayer hoppings, easier. With the hopping parameter choice discussed in Appendix A the band-structure along the k_x direction of the emerging BZ, with an area 4 (9) times smaller than that of the first (second) layer, is shown in Fig. 4(b). The dashed-magenta (solid-blue) lines correspond to the non-interacting (interacting) layers. In this example, the interaction between layers is introduced by using finite hopping matrix elements between layers. Details on which particular hoppings are introduced and their values are given in Appendix A. Notice that allowing for interlayer couplings through interlayer hoppings some of the degeneracies at the BZ boundaries are lifted opening gaps (Fig. 4(b)).

Notice that the band-structure shares a lot of the characteristics of our 1D example, with many mini-bands and mini-gaps produced by the BZ folding and the layer-layer interactions. The interlayer hoppings used here were rather large which leads to bands inside the original gap. Smaller values of these parameters will not affect as much the original gap.

C. Twisted bi-layers

As an example of twisted layers, we considered two atomically-thin layers of the same lattice discussed in the previous paragraph, i.e., a square lattice of atoms a with an atom b at the center of the square as shown in the left panel of Fig. 5(a), and we twisted one of them by an angle θ (in this example $\sin \theta = 4/5$) with respect to the first to obtain the structure shown in the right-panel of Fig. 5(a). When the rotated layer is placed on top of the first one, the pattern illustrated in Fig. 5(b) is produced with a super-lattice constant $a_s = \sqrt{5}a$.

The band-structure along the k_x direction of the small BZ of the moiré super-lattice obtained, as outlined in the Appendix B, is illustrated in Fig. 6(b). When we include weak interactions (see Sec. III), we obtain the blue-lines of the band-structure along the k_x direction of the small BZ of the moiré super-lattice shown in Fig. 6(b). The Brillouin zone of the twisted bilayer is shown in Appendix B. The band structures of each of the untwisted layers is also shown in Fig. 6(a) for comparison. The main features (many mini-bands and mini-gaps) of the band-structure are similar to those of the previous example.

III. ROLE OF INTERACTIONS

In this section we study the role of interactions a) on the tight-binding models introduced in the previous

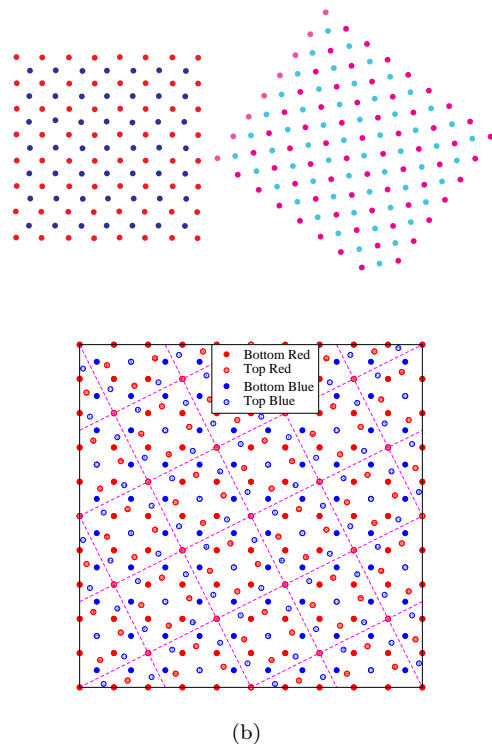


FIG. 5. (a) One layer (top left) and a second layer (top right) twisted by an angle θ (in this example $\sin \theta = 4/5$). (b) Moiré structure produced by placing the two layers on top of each other.

section and b) on the relaxation of the photo-excited electron-hole pairs.

A. On the tight-binding bands

In the previous Section, we have demonstrated that, as expected, the super-periodic structure formation leads to the folding of the BZ where along the mini-BZ edge gaps are expected to form because the interactions generally lift the degeneracies.

- The simplest form of interactions that can lift these degeneracies at the BZ edges is when we explicitly introduce non-zero matrix elements which couple the Bloch state $|n\mathbf{k}\rangle$ corresponding to band labeled n with the Bloch states $|n\mathbf{k} + \mathbf{G}\rangle$ (which in the folded BZ will require a different band index) for \mathbf{k} near the mini-BZ boundary defined by the reciprocal lattice vectors \mathbf{G} . This approach was implemented in the mismatched chains in Sec. II A to find the transition from the TB bands to the interacting ones with gaps formed at the mini-BZ boundaries.
- Another simple way to include effects of interactions that can create gaps at the mini-BZ bound-

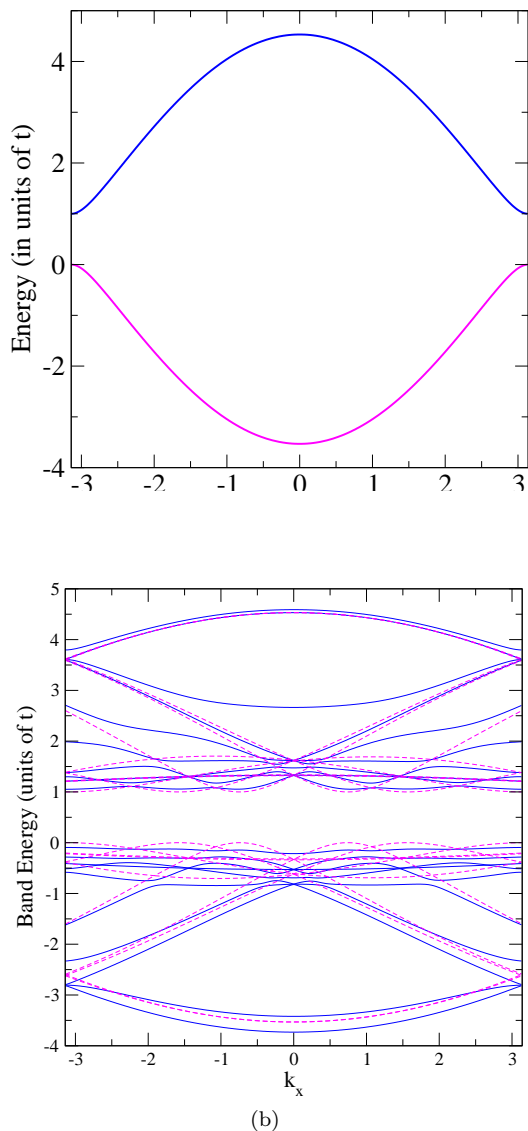


FIG. 6. (a) The band-structure of each of the two untwisted layers. (b) The band-structure of the twisted bilayer (Magenta (blue) lines denote non-interacting (interacting) layers).

aries is when we include interlayer hoppings. This was demonstrated in our tight-binding model for the lattice mismatched bilayer in Sec II B.

- The mini-bands have small bandwidth and, therefore, the effects of Coulomb interactions are expected to be significant. In order to schematically illustrate the role of the Coulomb interactions on the band-structure as described within the quantum lattice gas models defined by our tight-binding models of the previous section, we will confine our approach to a mean-field-like approximation. As an example, we will apply a Hartree-Fock-like approximation to include some effects of electron-electron interactions in the band structure of the twisted-

bilayer system introduced in Sec. II C.

However, application of the Hartree-Fock approximation[24] requires knowledge of the actual atomic orbitals (or Wannier states) in order to calculate the direct and exchange integrals of the Coulomb interaction. A generic tight-binding model defined on a given lattice, only specifies the hopping matrix elements between such states assumed to live on sites, but not explicitly these states (orbitals) themselves. To find those one needs to consider a specific material and carry out a DFT or, in general, a microscopic calculation with the same goal. Therefore, we will have to extend our TB model to one where the interactions are introduced also at the level of another model (such an example is the Hubbard model).

Our tight-binding model is a quantum lattice-gas model which consists of sites inside a supercell with index \mathbf{R}_s . Inside each such supercell N_o orbitals, specified with the index $\alpha = 1, \dots, N_o$, reside. After the TB calculation the Block states are written as

$$|\Psi_{n,\mathbf{k}}\rangle = \sum_{\alpha=1}^{N_o} c_{\alpha}^{(n)}(\mathbf{k})|\mathbf{k}, \alpha\rangle, \quad (2)$$

where

$$|\mathbf{k}, \alpha\rangle = \frac{1}{\sqrt{N_s}} \sum_{\mathbf{R}_s} e^{-i\mathbf{k}\cdot\mathbf{R}_s} |\mathbf{R}_s, \alpha\rangle, \quad (3)$$

and $|\mathbf{R}_s, \alpha\rangle$ represents the α orbital in the supercell specified by the lattice vector \mathbf{R}_s . The coefficients $c_{\alpha}^{(n)}(\mathbf{k})$ are found after the diagonalization of the $N_o \times N_o$ TB matrix for a given value of \mathbf{k} of the mini-BZ.

The Hartree-Fock Hamiltonian written in the basis of the atomic or (Wannier) states given by Eq. 3 in momentum space has the following form:

$$H_{\alpha\beta}(\mathbf{k}) = T_{\alpha\beta}(\mathbf{k}) + V_{\alpha\beta}(\mathbf{k}), \quad (4)$$

$$V_{\alpha\beta}(\mathbf{k}) = \sum_{\gamma,\mathbf{k}'} n_{\gamma}(\mathbf{k}') \left(U_{\alpha\mathbf{k}\gamma\mathbf{k}'\gamma\mathbf{k}'\beta\mathbf{k}} - U_{\alpha\mathbf{k}\gamma\mathbf{k}'\beta\mathbf{k}\gamma\mathbf{k}'} \right) \quad (5)$$

where

$$U_{\alpha_1\mathbf{k}_1\alpha_2\mathbf{k}_2\alpha_3\mathbf{k}_3\alpha_4\mathbf{k}_4} = \langle \mathbf{k}_1, \alpha_1, \mathbf{k}_2, \alpha_2 | U_c | \mathbf{k}_3, \alpha_3, \mathbf{k}_4, \alpha_4 \rangle \quad (6)$$

is the two-body matrix element of the Coulomb interaction between pairs of Wannier states given by Eq. 3 and Eq. 5 includes both the direct and the exchange terms. Here $T_{\alpha\beta}(\mathbf{k})$ is the TB matrix which was diagonalized in the previous section in order to obtain the non-interacting folded bands. The summation over γ is over occupied states, i.e., $n_{\gamma}(\mathbf{k})$ is the Fermi-Dirac distribution. The starting tight-binding model is a general model in which only the hopping matrix elements between sites are specified and the atomic or more generally the Wannier orbitals that correspond to the sites are not specified. Therefore, instead of starting by making a

model for these Wannier states and, then, calculating the matrix elements of U_c , we are going to make a model for the interaction matrix elements $V_{\alpha\beta}(\mathbf{k})$ directly. Thus, in order to schematically model the role of interactions on the band structure, we have used the following two different forms for such matrix elements:

$$V_{\alpha\beta}(\mathbf{k}') = V_0 \exp\left[-\left(\frac{E_{\beta\mathbf{k}}^{(0)} - E_{\alpha\mathbf{k}}^{(0)}}{\Gamma}\right)^2\right], \quad (7)$$

$$V_{\alpha\beta}(\mathbf{k}) = \frac{V_0}{1 + \left(\frac{E_{\beta\mathbf{k}}^{(0)} - E_{\alpha\mathbf{k}}^{(0)}}{\Gamma}\right)^2}. \quad (8)$$

Here $E_{\alpha\mathbf{k}}^{(0)}$ are the TB (non-interacting) energy bands and V_0 and Γ are energy scales. Both models state the expectation that electrons in bands which are close in energy interact more strongly and the parameter Γ gives the range of this interaction. We find that for small values of V_0 and/or large values of Γ both models give essentially the same results. Depending on how strongly or weakly localized the Wannier orbitals are, the dependence of these matrix elements on the band-energy difference can be weak or strong. Another factor which will influence this dependence is the screening effects as reflected in the dielectric function of the material.

We have carried out the diagonalization of our HF-like model. Notice that in the bands presented in Fig. 7(a) the interaction opens gaps near the mini-BZ edges. However, not all the degeneracies at the BZ boundaries are lifted within the HF approximation and some will remain in some ‘‘theoretically exact’’ treatment. Some of these degeneracies should be lifted through the electron-phonon interaction by allowing the superlattice to relax. If the interactions are weak, the gap-openings take place only in the vicinity of the mini-BZ edges and do not become global gaps, i.e., through the entire BZ; they only lead to a depression of the density of states (DOS) in the vicinity of the band energy at the mini-BZ edges as illustrated in Fig. 7(b). Some gaps form in the DOS, but more generally a depression in DOS appears. Our DOS share very similar features as the HF calculation of Ref. [24] for twisted bilayer graphene, with the notable difference that graphene has no gap while our model for a general semiconductor parent material does have a gap. When the interaction is stronger as shown in Fig. 8(a) for $V_0/t = 0.2$ the gaps at the mini-BZ edges become larger and as shown in Fig. 8(b) the depressions of the DOS near the band energy of the mini-BZ edges becomes deeper.

In the following subsection, we will argue that these small (partial) gaps lead to enhancement of the PV efficiency because they limit the phase space for relaxation of the photo-excited electron-hole pairs via phonon emission. This reduces the rate of phonon emission which allows the impact ionization processes to take place as discussed in the next subsection.

B. On the relaxation of the photo-excitations

Now, let us consider the various interaction processes which take place in the photo-excited electron/hole system in an insulator with a band-structure in which the conduction and/or the valence bands have been fragmented by a multitude of small partial or full energy gaps created by either of the mechanisms discussed in the previous subsection.

We will consider the role of the interaction between the photo-excited electrons and holes with a) phonons, b) other electrons and holes, and c) with the incident solar photons. These interactions lead to a dynamic quasi-equilibrium state which leads to a finite photo-current. We are ultimately interested in finding the efficiency of converting the energy of the solar radiation into electrical energy.

First, the photo-excited electron/hole pairs can transfer energy to phonons through the phonon-emission process illustrated in Fig. 9(a) or a cascade of such processes:

$$e \leftrightarrow e' + \Gamma, \quad (9)$$

where Γ denotes the emitted phonon of momentum \vec{q} and polarization λ . The initially photo-excited electron state e decays to another electronic state e' of a different energy and momentum by emitting a phonon or multi-phonons. The decay rate of such processes can be estimated by

$$\frac{1}{\tau_{\vec{k}n}^{phonon}} = \sum_{\vec{q},\lambda} |M_{\nu\nu'\lambda}(\vec{k},\vec{q})|^2 \delta(\omega - (E_{\nu}(\vec{k}) - E_{\nu'}(\vec{k} - \vec{q}) - \hbar\omega_q^{(\lambda)}), \quad (10)$$

where $M_{\nu\nu'\lambda}(\vec{k},\vec{q})$ is the electron-phonon interaction vertex and $E_{\nu}(\mathbf{k})$, and $\omega^{(\lambda)}(\mathbf{q})$ are the electron-band energy and phonon frequencies. This decay rate of the excited electron or hole when ω is within the spectrum of the solar radiation is of the order of $10^{12} - 10^{13}/\text{sec}$ for the typical case of Si as calculated from first principles[25]. As we shall see this can be much smaller than the impact ionization rate (IIR) as the latter involves much larger energy scales related to the much stronger Coulomb interaction. Even when the created small gaps δG are of the order of 0.05 eV or even somewhat larger in the insulators considered here, they can be sufficiently large to reduce or stop the decay via the process described by Eq. 9 and illustrated in Fig. 9(a). The reason is that the phase space which allows such transitions gets significantly reduced because the phonon energies $\hbar\omega_q^{(\lambda)}$ are smaller (less than ~ 0.05 eV) to that needed to take enough energy from the electron to allow it to decay to a lower electronic state separated from its present state by this small gap, because $\hbar\omega_q^{(\lambda)} < \delta G$. The vertex (matrix element) of an electron emitting multiple phonons at the same time is very small, therefore, the decay has to be done with successive single phonon emission processes and each one will have a probability significantly less than unity because of the small gap.

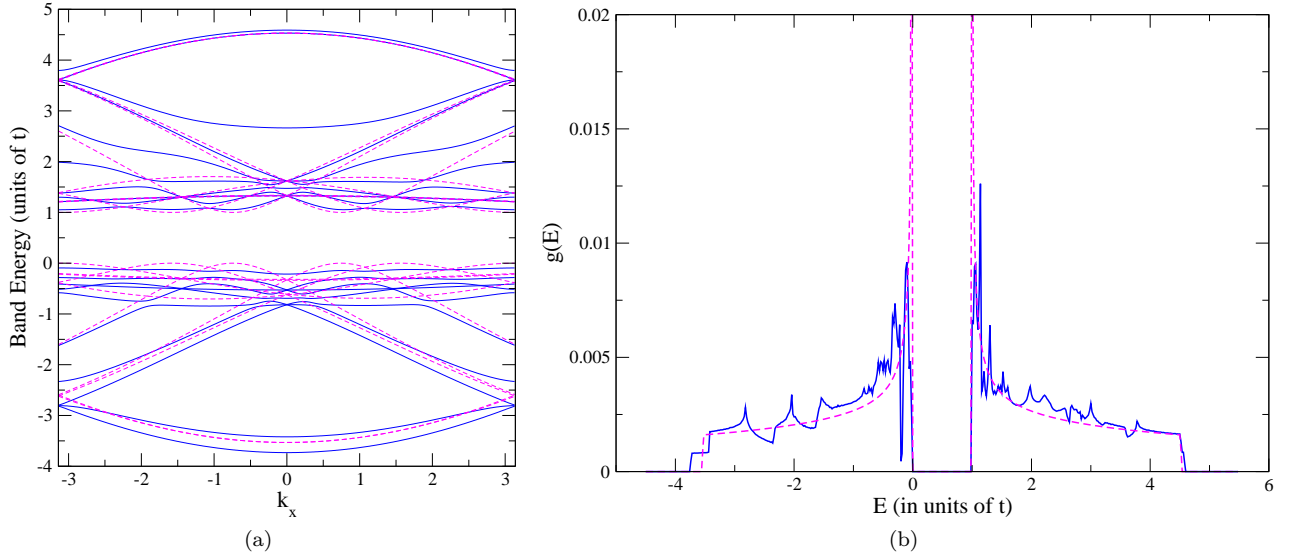


FIG. 7. (a) The bands of the twisted bilayer after the inclusion of the interaction discussed in the text for $V_0/t = 0.1$. (b) The density of states of the interacting twisted bilayer (blue solid line) is compared to that of the non-interacting (magenta

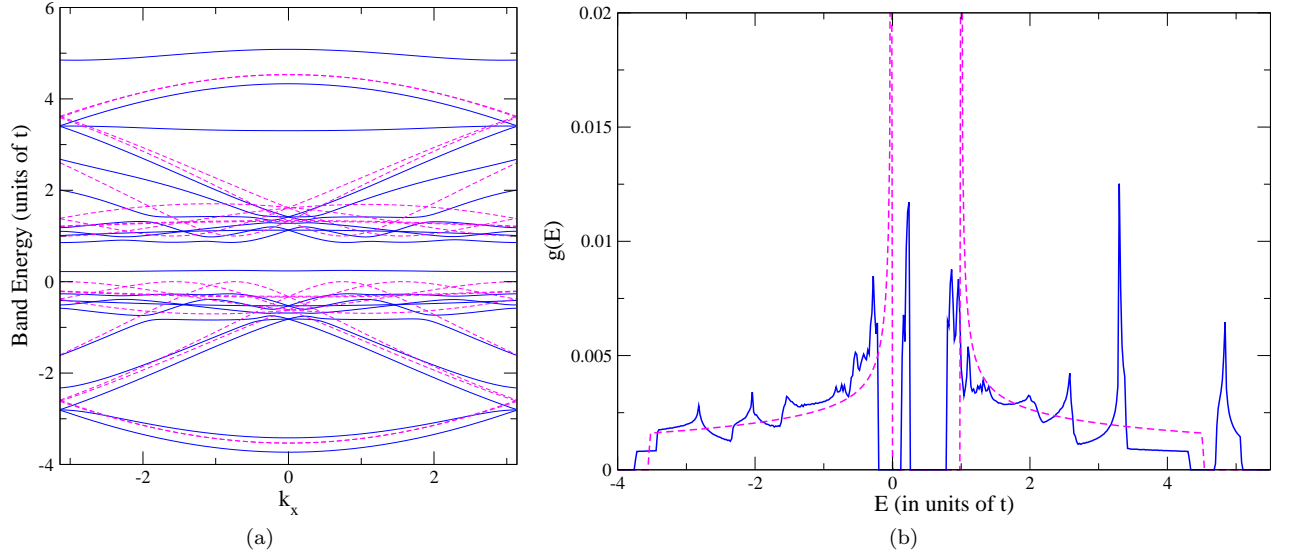


FIG. 8. (a) The bands of the twisted bilayer after the inclusion of the interaction discussed in the text for $V_0/t = 0.2$. (b) The density of states for $V_0/t = 0.2$ (blue solid line) is compared to that of the non-interacting (magenta dashed-line).

Another process of decay is the so-called impact ionization process (IIP) shown in Fig. 9(b), which increases the number of charge carriers per absorbed phonon. In order to calculate the IIP rate we need to include the processes illustrated diagrammatically in Fig. 9(b), where the electron or the hole component of the photo-excited electron-hole pair decays into two-electron-one-hole or two-hole-one-electron states respectively[13, 26]. An estimate of the IIP rate can be obtained using the quasiparticle self-energy obtained from quasiparticle-self-consistent

GW (QscGW) calculations. Namely, the IIP rate $\tau_{\vec{k}n}^{-1}$ is calculated from the self-energy $\Sigma_{\vec{k}n}(\omega)$ as follows:

$$\frac{1}{\tau_{\vec{k}n}} = \frac{2Z_{\vec{k}n}}{\hbar} |\text{Im} \Sigma_{\vec{k}n}(\omega)|, \quad (11)$$

$$Z_{\vec{k}n} = \left(1 - \text{Re} \frac{\partial \Sigma_{\vec{k}n}(\omega)}{\partial \omega} \Big|_{\epsilon_{\vec{k}n}} \right)^{-1}, \quad (12)$$

where \vec{k} and n are k-point and band indices. When n band indices are running for valence bands, then, they

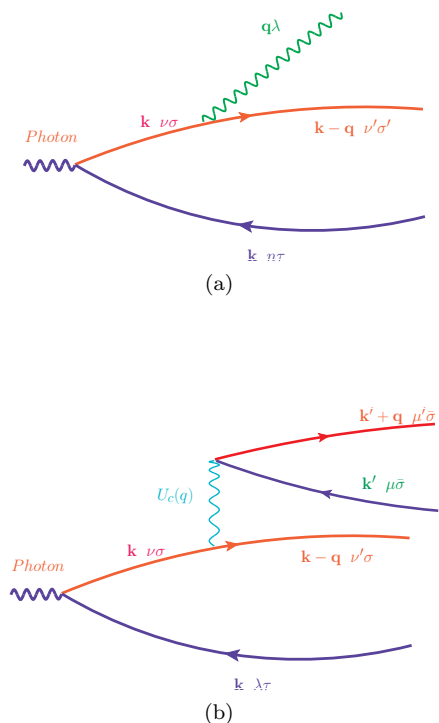


FIG. 9. (a) Within the photo-excited electron-hole pair the electron emits a phonon and, thus, decays from the state $\nu\mathbf{k}\sigma$ to the state $\nu'(\mathbf{k}-\mathbf{q})\sigma'$ by emitting a phonon of momentum \mathbf{q} , polarization λ and frequency $\omega_{\mathbf{q}}^{(\lambda)}$ (here ν and ν' are band labels). (b) Within the photo-excited electron-hole pair the electron interacts with a different valence electron and it promotes it to the conduction band, thus, leaving a hole behind. This is the process of the so-called impact ionization.

correspond to the recombination to the hole-initiated biexcitons, otherwise to the electron-initiated biexcitons. For the self-energy calculations, we use the same parameters as in the QscGW calculations mentioned earlier. This rate has been calculated[26] for insulators with flat bands, where the magnitude of the Coulomb interaction is much larger than their bandwidths, and it was found to be of the order of 10^{15} /sec in the spectrum of the solar radiation which is larger by 2 orders of magnitude as compared to the decay rate through phonon emission[25]. Therefore, IIP can dominate the energy relaxation processes in such materials. More importantly, the bands discussed in the previous section, have bands with bandwidths small compared to the magnitude of the Coulomb interaction because of the band-folding. Therefore, one expects an significantly increased IIP rate[26].

However, Auger recombination which is the inverse process should not be omitted. To analyze that, first, let us begin from the open-circuit situation. We have found[15] that for the type of insulators discussed in the previous section with flat bands, the characteristic time scale for thermalization of the photo-excited electrons and holes is much shorter than the time needed

for phonons to thermalize the electronic system with the lattice. Therefore, it is reasonable to assume that the photo-created electrons and the holes in these insulators thermalize among themselves at a temperature T_e higher than the lattice temperature T_L , by means of the electron-electron interaction. This interaction between the electronic degrees of freedom leads to processes such as impact ionization and Auger recombination, as well as carrier-carrier scattering. This equilibrium state is achieved as follows.

The quasi-equilibrium between the impact ionization process shown in Fig. 9(b) and the Auger recombination process, i.e., the inverse of the impact ionization process, shown as the reverse process of the one shown in Fig. 9(b), can be denoted as follows

$$e_1 \leftrightarrow e'_1 + e_2 + h, \quad (13)$$

where e_1 is the initial electronic state which interacts with a valence electron and promotes it to the conduction band, thus, creating an additional e-h pair denoted as e_2 - h , by changing its energy and momentum to become the state e'_1 . In addition, there is the analogous processes for high energy holes, i.e.,

$$h_1 \leftrightarrow h'_1 + e + h_2. \quad (14)$$

Last, the electron-electron scattering due to the Coulomb repulsion leads to electron-electron, hole-hole, and electron-hole interaction processes, which lead to the following quasi-equilibrium equations:

$$e_1 + e_2 \leftrightarrow e'_1 + e'_2, \quad (15)$$

$$h_1 + h_2 \leftrightarrow h'_1 + h'_2, \quad (16)$$

$$e + h \leftrightarrow e' + h'. \quad (17)$$

If these scattering processes are excluded, and we consider only impact ionization and Auger recombination, then, only those processes involving electrons and holes in certain energy and momentum range (which allow for impact ionization and its inverse through energy-momentum conservation) would take place and everything else would be excluded. As a result, the final distribution of carriers would depend on energy and momentum and, thus, it cannot be described by a Fermi-Dirac distribution. We would like to remind the reader that we have neglected the effects of electron-phonon interaction because, as we have shown, they lead to equilibrium with the lattice at a temperature T_L at a much longer time-scale. The above electronic scattering processes are important in order to establish a quasi-equilibrium of the electronic degrees of freedom at a common temperature T_e much higher than T_L and the electron/hole distribution becomes a Fermi-Dirac distribution with characteristic temperature T_e . Therefore, these scattering processes are absolutely important and we include them as part of the mechanism which leads to the fast electronic quasi-equilibrium.

IV. EQUILIBRIUM AND PV-EFFICIENCY

We consider a “parent” bulk material that consists of valence and conduction bands with bandwidths W_v and W_c separated by a relatively large gap E_g . In addition, W_v and W_c are larger than 3.5 eV, the approximate upper bound of the solar radiation spectrum. We will assume that, through either of the two mechanisms discussed in the previous section (lattice mismatched or twisted layers), these large bands split into many bands with smaller bandwidths δW and small gaps δG . In order to be concrete we consider a simplified but quite general model for the energy bands. We will assume that the overall density of states of the parent bulk semiconducting material used to make these superlattice structures does not change, only small gaps open, creating the following energy bands and gaps:

$$E_n^{(b)} = E_g + (n-1)(\Delta W + \delta G), \quad (18)$$

$$E_n^{(t)} = E_n^{(b)} + \Delta W. \quad (19)$$

where $n = 1, 2, \dots, M$. First, there is a relative large gap E_g , i.e., the gap in the original bulk semiconductor. The band-folding, due to the super-structure formation from the lattice mismatch or the moiré periodicity, causes the opening of small gaps δG which split the original conduction band.

This model is a simplified version of what actually happens in the actual material as discussed in the previous section. However, here, what we wish to show is the following: These additional gaps prevent absorption of the solar radiation when the energy of the incident photon falls within these gaps. Therefore, naively, one would expect a reduced PV efficiency. However, as we argued in the previous section these small gaps prevent energy loss via phonon emission and enhance the rate of IIP. Next, we will show that the overall effect is to significantly enhance the PV efficiency, especially in the limit of very small gaps.

To begin, the flux of the incident solar radiation creates the energy current of the absorbed solar photons given by

$$J_{absorbed} = \frac{\Omega_s}{4\pi^3 \hbar^3 c^2} \sum_{n=1}^M \int_{E_n^{(b)}}^{E_n^{(t)}} d\epsilon \frac{\epsilon^3}{\exp(\frac{\epsilon}{k_B T_s}) - 1}, \quad (20)$$

where Ω_s is the solid angle under which the Sun is seen, and T_s is the Sun’s surface temperature $T_s \simeq 5760$ K. Here, the incident radiation is not absorbed when the photon energy falls within any of the band gaps.

If we now consider the equilibrium of all of the processes discussed in the previous section, we may realize that they produce a distribution of electron/hole pairs in quasi-equilibrium with the distribution of photons over energy due to the emission process:

$$e + h \leftrightarrow \gamma. \quad (21)$$

in which an electron (e) and a hole (h) combine and a photon (γ) is emitted (luminescence) or the inverse where

a photon produces an electron/hole pair in these insulators. This distribution of photons in equilibrium with a gas of quasiparticles consisted of electrons and holes can be described by a thermal distribution of photons at a temperature T_e and a chemical potential $\mu_\gamma = \mu_{e-h} = 0$. The value of T_e is determined from the equation

$$J_{emitted} = J_{absorbed}, \quad (22)$$

$$J_{emitted} = \frac{\Omega_e}{4\pi^3 \hbar^3 c^2} \sum_{n=1}^M \int_{E_n^{(b)}}^{E_n^{(t)}} d\epsilon \frac{\epsilon^3}{\exp(\frac{\epsilon - \mu_\gamma}{k_B T_e}) - 1}. \quad (23)$$

Here Ω_e is the solid angle of the emitter and it is π for a planar emitter. This equation defines a temperature T_e of the electronic system which is considered decoupled from the lattice and the phonons. A value of $\mu_{e-h} = 0$ is expected for a system in which the particle number is not conserved as is the case for the electron and holes in the equilibrium state determined by the impact ionization and Auger-recombination.

If we assume that the density of the electrons and of holes near the interface of the PV junction is not large, the above process produces an quasi-equilibrium Fermi-Dirac distribution of electrons and holes at the above temperature T_e with no separation of the quasi-Fermi-energies, i.e, the chemical potential difference between electron and holes μ_{e-h} is zero.

Under open circuit conditions, this quasi-equilibrium is achieved at the temperature T_e , which is higher than the lattice temperature T_L . As discussed in the previous section, the time scale in these insulators to reach equilibrium (through impact ionization, Auger recombination and electron-electron scattering) is much shorter than the time scale required for such a system to reach thermal equilibrium with the lattice through the process described by Eq. 9 and the following process

$$e + h \leftrightarrow \Gamma, \quad (24)$$

where Γ denotes a phonon. This happens because

- the time-scale for the decay processes described by Eqs. 13 and 14 is much faster than the process of electron decay via phonons and
- the interaction matrix elements involved in the processes described by Eq. 15, 16,17 are much stronger than the electron-phonon interaction matrix elements leading to the processes 24.

These facts allow first equilibration of the electronic system to a temperature T_e , which is different than T_L by creating multiple electron-hole carriers per incident photon. This phenomenon has been argued in Refs. 27–29 to lead to a significant increase of the efficiency by means of carrier multiplication [28] for a conventional solar cell.

With these facts in mind, we treated the carriers in the insulator as weakly interacting quasiparticles which obey Fermi-Dirac statistics, which may allow us to apply the

same assumptions and approximations used by Brendel et al.[28] to calculate the efficiency of a solar cell made from the material characterized by the band structure described by Eq. 19. We find that the maximum efficiency is bounded from above by the maximum of the following function of the voltage V and the gaps δG :

$$\eta(V) = qV \frac{G - R(V)}{P_{in}}, \quad (25)$$

where q is the carrier charge and we are seeking the maximum of $\eta(V)$ with respect to the voltage V . P_{in} is the incident solar radiation power given by

$$P_{in} = \kappa_s \int_0^\infty d\epsilon \frac{\epsilon^3}{\exp(\epsilon/k_B T_s) - 1}, \quad (26)$$

where the $\kappa_s = e_s \frac{2}{c^2 \hbar^3}$ and $e_s = \pi A \sin^2 \phi_s$ is the illumination étendue[1] of a cell of area A that sees the Sun under a half angle ϕ_s . As already mentioned, T_s is the temperature on the solar surface.

The quantity G is the generation current given by

$$G = \kappa_s \sum_{n=1}^{\infty} \int_{E_n^{(b)}}^{E_n^{(t)}} d\epsilon \frac{m(\epsilon) \epsilon^2}{\exp(\epsilon/k_B T_s) - 1}, \quad (27)$$

$m(\epsilon) = \min([\frac{\epsilon}{E_g}], m_{\max})$ is the number of electron-hole pairs[28] generated by one hot carrier of energy ϵ through the process of impact ionization, where $[\frac{\epsilon}{E_g}]$ stands for the integer part and m_{\max} is a maximum allowed value of the carrier multiplication.

$R(V)$ is the electron-hole recombination current which produces photons or due to the Auger process current (the inverse process of the process illustrated in Fig.9(b)). The result is a recombination current given as

$$R(V) = \kappa_s \xi \sum_{n=1}^{\infty} \int_{E_n^{(b)}}^{E_n^{(t)}} d\epsilon \frac{m(\epsilon) \epsilon^2}{\exp((\epsilon - qV)/k_B T_e) - 1} \quad (28)$$

where $\xi = \pi/\Omega_s$ and $\xi = 46396$ ($\xi = 1$) corresponds to unconcentrated (fully concentrated) sunlight.

In Fig. 10, the calculated efficiency is shown for $\delta G = 0.05eV$ and $\delta E = 0.5eV$ for the case of unconcentrated sunlight for various values of m , which is the number of electron-hole pairs allowed to be generated by a single solar photon when it has sufficient energy through the process of impact ionization (see Ref. [28]). The red-dashed line in Fig. 10 shows the result of the $\delta G = 0$ and $m = 1$ which yields the Shockley-Queisser (SQ) result. Notice that the corresponding result for $m = 1$ but with $\delta G = 0.05 eV$ is somewhat lower than the one for $\delta G = 0$, as expected as some photons go through the gaps. However, splitting the bands allows for impact-ionization to occur, i.e., m can be greater than 1. As a result we see that regardless of the fact that some photons are going through the gaps, for $m = 2$ (magenta) and $m = 4$ (blue) the efficiency is significantly higher than the SQ result. Therefore, this calculation contrary to naive expectations

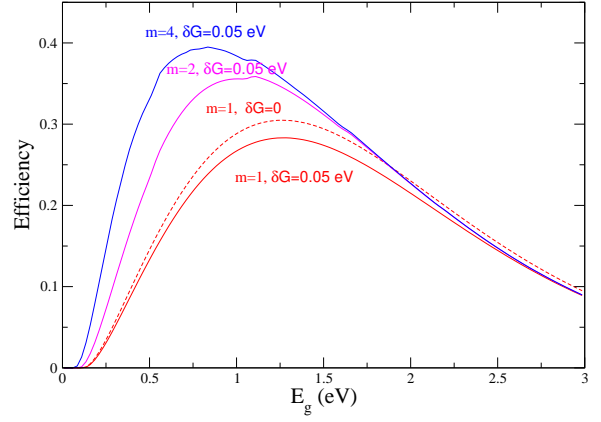


FIG. 10. Calculated efficiency ($\delta G = 0.05eV$, $\delta E = 0.5eV$) for unconcentrated light. Here m is the number of electron-hole pairs allowed to be generated by a single solar photon (when it has sufficient energy) through the process of impact ionization (Fig. 12(b-c)).

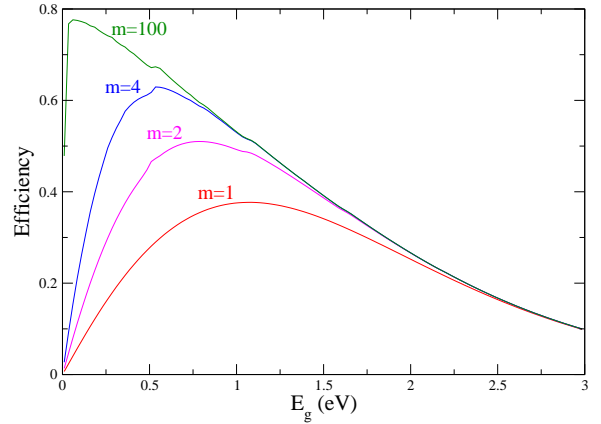


FIG. 11. Calculated efficiency ($\delta G = 0.05eV$, $\delta E = 0.5eV$) for fully concentrated sun-light.

strongly suggests that opening small gaps in the electronic spectrum can enhance the PV efficiency. Namely, while the PV cell would miss those photons which have the energy to go through the gap, the net efficiency increases because these gaps allow for the impact ionization process to occur.

In Fig. 11, the calculated efficiency is shown for $\delta G = 0.05eV$ and $\delta E = 0.5eV$ for the case of fully concentrated sunlight ($\xi = 1$) and for various values of m . Notice the dramatic increase in efficiency due to carrier multiplication in this case, especially in the limit of vanishingly small gap and allowing for the impact ionization process to work for arbitrarily large but energetically possible values of m .

V. DISCUSSION AND CONCLUSIONS

We have calculated the PV efficiency enhancement when a semiconductor band splits into multiple bands with small bandwidths separated by small gaps by extending the work of Shockley-Queisser[1] and by including the effects of impact ionization which as we show becomes much more probable in this case. Realization of this case can be found in alternating-layer structures of lattice mismatched or misaligned (twisted) atomically-thin layers. We show that there is a significant efficiency enhancement as compared to the SQ limit in the case where the band is split, because in such case a) the electron or hole decay rate through phonon emission is reduced because of the mini-gaps, and b) the impact ionization rate should be significantly increased because the bands become flat[15] and because of reduced probability for carrier decay through phonon emission. The impact ionization process leads to multiple carrier generation.

Namely, we find that the process of decay via phonon emission is halted by the presence of the minigaps in our proposed structures until the excited electron finds a hole to recombine or excites another electron from the valence band through the process of impact ionization. Namely, the fragmented conduction and valence bands work as a catalyst for impact ionization, because the small gaps block the decay channel through phonons of the photoexcited electrons and holes.

In a nutshell the mechanism can be described in simple terms as follows: First, in the absence of band fragmentation, when the band-structure is as the one illustrated in Fig. 12(a), the incident solar photon promotes an electron from the valence band to the conduction band significantly above the CBM. Subsequently, the electron decays to the CBM via a series phonon emission processes. In such case the excess energy, beyond the large energy gap, is consumed by phonons, which leads to a significant limitation of the PV efficiency[1]. In the case of band fragmentation (Fig. 12(b)), when the same incident solar photon promotes an electron to a high-energy mini-band n with energy $E_n(\mathbf{k})$, and bandwidth W_n , separated by the lower energy band $n - 1$ by a gap G_n , the excited electron can only lose a small part of its energy by emitting phonons. The presence of the small gap G_n , between successive bands, prevents further phonon emission. Furthermore, the mechanisms left for the electron to lose more energy are only a) recombination with a hole or b) to fall into a lower energy band and simultaneously promote another valence electron to a low energy band. This second process (illustrated in Fig. 12(c)) is the well-known impact ionization process which leads to multi-carrier generation[13–15]. The photon produced by process (a) of recombination can also generate a different electron/hole pair, also leading to carrier multiplication, thus, increasing efficiency further. We have not included this latter efficiency increasing process[30]. We have included, however, in addition to the impact ionization and Auger recombination processes, the role of

carrier recombination, and of electron-electron, hole-hole and electron-hole scattering.

For completeness we would like to mention that for reasons somewhat related to what is proposed here, some time ago, it was suggested that using confining geometries, such as quantum wells, quantum wires, quantum dots and nanostructures, the relaxational time scales can be significantly affected [10–12, 31] which would allow the possibility for impact ionization.

In conclusion, we have demonstrated that splitting the bands by means of growing multilayers of alternating lattice-mismatched atomically-thin layers of semiconductors or by means of alternating twisted multilayers of the same atomically-thin layers, can lead to a significant improvement in the efficiency of converting the broad solar spectrum into electrical energy.

VI. ACKNOWLEDGMENTS

This work was supported by the U.S. National Science Foundation under Grant No. NSF-EPM-2110814.

Appendix A: Tight-binding treatment of the strained 3×3 bilayer

In this part of the appendix, we define the tight-binding matrix elements of the case of the strained (mismatched) 3×3 bilayer. We will use Fig. 13 to define the various hopping matrix elements of our tight-binding model.

For the bottom layer (layer 1) we use on-site energies for the black and blue sites: $E_B = 0$ $E_b = 1.0$ eV. We only consider the hopping matrix element between black and its four diagonally neighboring blue sites and we take it to be $t = 1$ eV.

Similarly for the top layer (layer 2) there are white and red sites with on-site energies: $E_W = 0$ $E_R = 1.0$ eV. The white sites form a square lattice of lattice constant $a' = 2/3a$ with a red site in the center. The only hopping matrix element in the second layer is between white and its four diagonally neighboring red sites and we take it as $t' = 0.5$ eV.

We introduce the following interlayer hopping matrix elements. When a white site is exactly on top of a black site there is a hopping $t_0 = 0.4$ eV. When a red site is exactly on top of a black site there is a hopping $t'_0 = 0.4$ eV. We allow a hopping matrix element of $t_1 = 0.3$ eV between a black and the nearest white site (which is either along the x or y direction relative to the black site, such as W_2 and B_2 sites or B_3 and W_7 sites in Fig. 13). Similarly we allow a hopping $t'_1 = 0.3$ eV between a black and the nearest red site (which is either along the x or y direction relative to the black site, such as B_2 and R_2 sites or B_3 and R_4 sites in Fig. 13). Moreover, a hopping $t_2 = 0.2$ eV is used between a black and the nearest red site (which is at 45° relative to the black site, such as

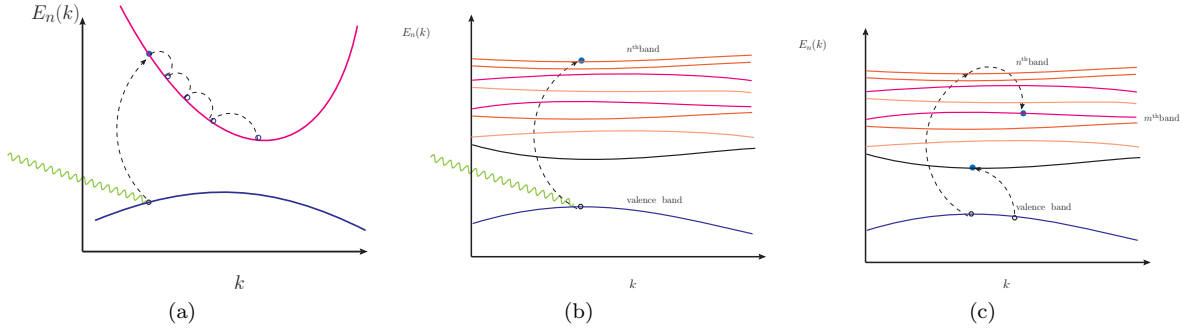


FIG. 12. See main text for explanation.

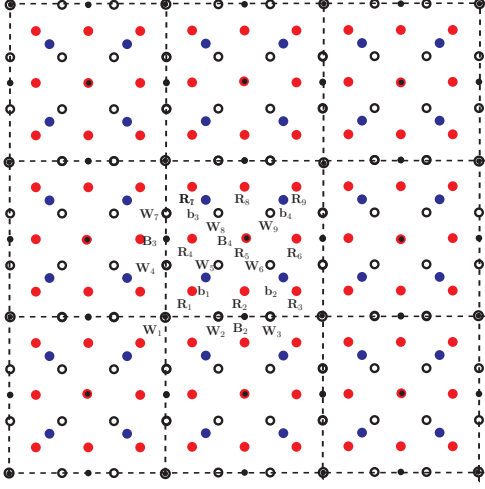


FIG. 13. The same lattice as the one of Fig. 3(b) where we have marked the atoms in order to define the matrix elements of Table I

B_1 and R_1 sites in Fig. 13). A hopping matrix element $t'_2 = 0.2$ eV is used between a black and the nearest white sites (which is at 45° relative to the black sites, such

as B_4 and W_5 sites in Fig. 13). A hopping $t_3 = 0.3$ eV between a blue and the nearest white site (which is at 45° relative to the black site, such as b_1 and W_5 sites or b_3 and W_8 sites in Fig. 13) is used. Lastly, we use a hopping $t_4 = 0.3$ eV between a blue and the nearest red site (which is at 45° relative to the black site, such as b_1 and R_1 sites or b_3 and R_7 sites in Fig. 13).

These matrix elements lead to the tight-binding matrix in momentum space given in Table I.

Our results of the diagonalization of this matrix for the parameter values discussed above lead to the band structure discussed in the main part of the paper.

Appendix B: Brillouin zone of twisted bilayer

The moiré BZ is shown in the right panel of Fig. 14, along with those of each individual layer. When we fold the 2 bands of each layer inside the moiré BZ, as schematically illustrated in Fig. 14, we obtain the non-interacting bands shown by broken magenta lines in Fig. 6(b) of the main manuscript. Fig. 14(b) shows the moiré BZ is expanded in the 4 directions using 4 reciprocal lattice vectors. Fig. 14(c) demonstrates that the BZ moiré BZ and its 4 extensions cover completely the large BZ of the bottom layer by cutting and pasting the pieces 1,2,3,4.

-
- [1] W. Shockley and H. J. Queisser, Detailed Balance Limit of Efficiency of p-n Junction Solar Cells, *Journal of Applied Physics* **32**, 510 (1961), <https://pubs.aip.org/aip/jap/article-pdf/32/3/510/18323491/51010101.pdf>.
- [2] M. Yamaguchi, F. Dimroth, J. F. Geisz, and N. J. Ekins-Daukes, Multi-junction solar cells paving the way for super high-efficiency, *Journal of Applied Physics* **129**, 240901 (2021), <https://pubs.aip.org/aip/jap/article-pdf/doi/10.1063/5.0048653/16783250/240901-1.pdf>.
- [3] Y. H. Lee, Beyond the shockley-queisser limit: Exploring new frontiers in solar energy harvest, *Science* **383**, eado4308 (2024).
- [4] W. Walukiewicz, W. Shan, K. M. Yu, J. W. Ager, E. E. Haller, I. Miotkowski, M. J. Seong, H. Alawadhi, and A. K. Ramdas, Interaction of localized electronic states with the conduction band: Band anticrossing in ii-vi semiconductor ternaries, *Phys. Rev. Lett.* **85**, 1552 (2000).
- [5] W. Walukiewicz, J. W. Ager, E. E. Haller, J. F. Geisz, D. J. Friedman, J. M. Olson, and S. R. Kurtz, Band anticrossing in gainnas alloys, *Phys. Rev. Lett.* **82**, 1221 (1999).
- [6] N. López, L. A. Reichertz, K. M. Yu, K. Campbell, and J. F. Geisz, Engineering the electronic band structure for multiband solar cells, *Phys. Rev. Lett.* **106**, 028701 (2011).
- [7] Y. Okada, N. J. Ekins-Daukes, T. Kita, R. Tamaki, M. Yoshida, A. Pusch, O. Hess, C. C. Phillips, D. J. Farrell, K. Yoshida, N. Ahsan, Y. Shoji, T. Sogabe, and J.-F. Guillemoles, Intermediate

	B_1	B_2	B_3	B_4	W_1	W_2	W_3	W_4	W_5	W_6	W_7	W_8	W_9	R_1	R_2	R_3	R_4	R_5	R_6	R_7	R_8	R_9	b_1	b_2	b_3	b_4
B_1	E_B	0	0	0	0	0	0	0	0	0	0	0	0	t_1	0	t_1^{-x}	0	0	0	t_1^{-y}	t	t^{-x-y}	t	t^{-x}	t^{-y}	t^{-x-y}
B_2	0	E_B	0	0	0	0	t_2	t_2	0	0	0	0	0	t_1	0	t_1^{-x}	0	0	0	t_1^{-y}	t	t^{-x-y}	t	t^{-x}	t^{-y}	t^{-x-y}
B_3	0	0	E_B	0	0	0	0	t_1	0	0	t_1	0	0	0	0	t_1^{-x}	0	t_1^{-y}	0	0	0	0	t	t^{-x}	t	t^{-x}
B_4	0	0	0	E_B	0	0	0	0	t_1	t_1	0	t_1	t_1	0	0	0	0	t_0'	0	0	0	0	t	t	t	t
W_1	t_0	0	0	0	E_W	0	0	0	0	0	0	0	0	t'	0	t'^{-x}	0	0	0	t'^{-y}	0	t'^{-x-y}	0	0	0	0
W_2	0	t_1	0	0	0	E_W	0	0	0	0	0	0	0	0	t'	0	0	0	0	t'^{-y}	t'^{-y}	0	0	0	0	0
W_3	0	t_1	0	0	0	0	E_W	0	0	0	0	0	0	0	t'	t'	0	0	0	0	t'^{-y}	t'^{-y}	0	0	0	0
W_4	0	0	t_1	0	0	0	0	E_W	0	0	0	0	0	t'	0	t'^{-x}	t'	0	t'^{-x}	0	0	0	0	0	0	0
W_5	0	0	0	t_2'	0	0	0	0	E_W	0	0	0	0	t'	t'	0	t'	t'	0	0	0	0	t_3	0	0	0
W_6	0	0	0	t_2'	0	0	0	0	0	E_W	0	0	0	0	t'	t'	0	t'	t'	0	0	0	0	t_3	0	0
W_7	0	0	t_1	0	0	0	0	0	0	0	E_W	0	0	0	0	0	t'	0	t'^{-x}	t'	0	t'^{-x}	0	0	0	0
W_8	0	0	0	t_2'	0	0	0	0	0	0	0	E_W	0	0	0	0	t'	t'	0	t'	t'	0	0	0	t_3	0
W_9	0	0	0	t_2'	0	0	0	0	0	0	0	0	E_W	0	0	0	0	t'	t'	0	t'	t'	0	0	0	t_3
R_1	t_2	0	0	0	t'	t'	0	t'	t'	0	0	0	0	E_R	0	0	0	0	0	0	0	0	t_4	0	0	0
R_2	0	t_1'	0	0	0	t'	t'	0	t'	t'	0	0	0	0	E_R	0	0	0	0	0	0	0	0	0	0	0
R_3	t_2^{+x}	0	0	0	t'^{+x}	0	t'	t'^{+x}	0	t'	0	0	0	0	0	E_R	0	0	0	0	0	0	0	t_4	0	0
R_4	0	0	t_1'	0	0	0	0	t'	t'	0	t'	t'	0	0	0	0	E_R	0	0	0	0	0	0	0	0	0
R_5	0	0	0	t_0'	0	0	0	0	t'	t'	0	t'	t'	0	0	0	0	E_R	0	0	0	0	0	0	0	0
R_6	0	0	$t_1'^{+x}$	0	0	0	0	t'^{+x}	0	t'	t'^{+x}	0	t'	0	0	0	0	0	E_R	0	0	0	0	0	0	0
R_7	t_2^{+y}	0	0	0	t'^{+y}	t'^{+y}	0	0	0	0	t'	t'	0	0	0	0	0	0	0	E_R	0	0	0	0	t_4	0
R_8	0	$t_1'^{+y}$	0	0	0	t'^{+y}	t'^{+y}	0	0	0	0	t'	t'	0	0	0	0	0	0	0	E_R	0	0	0	0	0
R_9	t_2^{+x+y}	0	0	0	t'^{x+y}	0	t'^{+y}	0	0	0	t'^{+x}	0	t'	0	0	0	0	0	0	0	0	E_R	0	0	0	t_4
b_1	t	t	t	t	0	0	0	0	t_3	0	0	0	0	t_4	0	0	0	0	0	0	0	0	E_b	0	0	0
b_2	t^{+x}	t	t^{+x}	t	0	0	0	0	0	t_3	0	0	0	0	0	0	0	0	0	0	0	0	0	E_b	0	0
b_3	t^{+y}	t^{+y}	t	t	0	0	0	0	0	0	0	t_3	0	0	0	0	0	0	0	0	t_4	0	0	0	E_b	0
b_3	t^{x+y}	t^{+y}	t^{+x}	t	0	0	0	0	0	0	0	0	t_3	0	0	0	0	0	0	0	0	0	t_4	0	0	E_b

TABLE I.

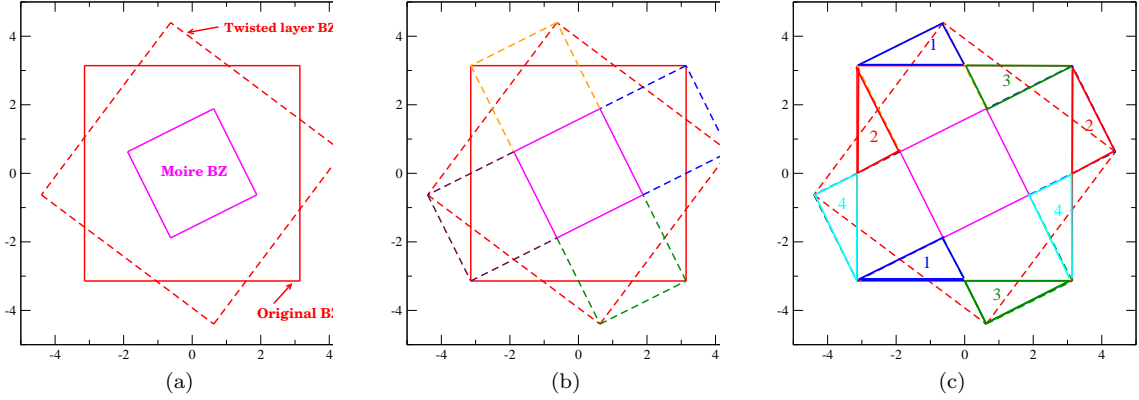


FIG. 14. (a) The large-size Brillouin zones shown are those of each of the layers, while the smaller-size Brillouin zone corresponds to the combined moiré-structure. (b) The moiré BZ is expanded in the 4 directions using 4 reciprocal lattice vectors. (c) Demonstration that the BZ moiré BZ and its 4 extensions cover completely the large BZ of the bottom layer by cutting and pasting the pieces 1,2,3,4.

- band solar cells: Recent progress and future directions, *Applied Physics Reviews* **2**, 021302 (2015), <https://pubs.aip.org/aip/apr/article-pdf/doi/10.1063/1.4916561/14573461/0213021um.pdf>
- [8] A. Luque and A. Martí, Increasing the efficiency of ideal solar cells by photon induced transitions at intermediate levels, *Phys. Rev. Lett.* **78**, 5014 (1997).
- [9] T. Iqbal, S. Fatima, T. Bibi, and M. Zafar, Graphene and other two-dimensional materials in advance solar cells, *Optoelectronics and Communications* **53**, 228 (2021).
- [10] H. Benisty, C. M. Sotomayor-Torrès, and C. Weisbuch, Intrinsic mechanism for the poor luminescence properties of quantum-box systems, *Phys. Rev. B* **44**, 10945 (1991).

- [11] U. Bockelmann and G. Bastard, Phonon scattering and energy relaxation in two-, one-, and zero-dimensional electron gases, *Phys. Rev. B* **42**, 8947 (1990).
- [12] H. Benisty, Reduced electron-phonon relaxation rates in quantum-box systems: Theoretical analysis, *Phys. Rev. B* **51**, 13281 (1995).
- [13] E. Manousakis, Photovoltaic effect for narrow-gap mott insulators, *Phys. Rev. B* **82**, 125109 (2010).
- [14] J. E. Coulter, E. Manousakis, and A. Gali, Optoelectronic excitations and photovoltaic effect in strongly correlated materials, *Phys. Rev. B* **90**, 165142 (2014).
- [15] E. Manousakis, Optimizing the role of impact ionization in conventional insulators, *Scientific Reports* **9**, 20395 (2019).
- [16] L.-k. Shi, O. Matsyshyn, J. C. W. Song, and I. S. Vladiego, Berry-dipole photovoltaic demon and the thermodynamics of photocurrent generation within the optical gap of metals, *Phys. Rev. B* **107**, 125151 (2023).
- [17] T. G. Rappoport, T. A. Morgado, S. Lannebère, and M. G. Silveirinha, Engineering transistorlike optical gain in two-dimensional materials with berry curvature dipoles, *Phys. Rev. Lett.* **130**, 076901 (2023).
- [18] S. Zhang, L. Jin, Y. Lu, L. Zhang, J. Yang, Q. Zhao, D. Sun, J. J. P. Thompson, B. Yuan, K. Ma, Akriti, J. Y. Park, Y. H. Lee, Z. Wei, B. P. Finkenauer, D. D. Blach, S. Kumar, H. Peng, A. Mannodi-Kanakkithodi, Y. Yu, E. Malic, G. Lu, L. Dou, and L. Huang, Square moiré superlattices in twisted two-dimensional halide perovskites (2023), arXiv:2312.16679 [cond-mat.mtrl-sci].
- [19] Y. Cao, V. Fatemi, A. Demir, S. Fang, S. L. Tomarken, J. Y. Luo, J. D. Sanchez-Yamagishi, K. Watanabe, T. Taniguchi, E. Kaxiras, R. C. Ashoori, and P. Jarillo-Herrero, Correlated insulator behaviour at half-filling in magic-angle graphene superlattices, *Nature* **556**, 80 (2018).
- [20] Z. Li, J. Zhuang, L. Chen, Z. Ni, C. Liu, L. Wang, X. Xu, J. Wang, X. Pi, X. Wang, Y. Du, K. Wu, and S. X. Dou, Observation of van hove singularities in twisted silicene multilayers, *ACS Central Science* **2**, 517 (2016).
- [21] G. Sánchez-Santolino, V. Rouco, S. Puebla, H. Aramberri, V. Zamora, M. Cabero, F. A. Cuellar, C. Munuera, F. Mompean, M. Garcia-Hernandez, A. Castellanos-Gomez, J. Íñiguez, C. Leon, and J. Santamaria, A 2d ferroelectric vortex pattern in twisted batio3 freestanding layers, *Nature* **626**, 529 (2024).
- [22] S. Lee, D. J. P. de Sousa, B. Jalan, and T. Low, Moiré polar vortex, flat bands and lieb lattice in twisted bilayer batio₃ (2024), arXiv:2405.06132 [cond-mat.mtrl-sci].
- [23] J. Hagel, S. Brem, J. A. Pineiro, and E. Malic, Impact of atomic reconstruction on optical spectra of twisted tmd homobilayers, *Phys. Rev. Mater.* **8**, 034001 (2024).
- [24] T. Cea, N. R. Walet, and F. Guinea, Electronic band structure and pinning of fermi energy to van hove singularities in twisted bilayer graphene: A self-consistent approach, *Phys. Rev. B* **100**, 205113 (2019).
- [25] M. Bernardi, D. Vigil-Fowler, J. Lischner, J. B. Neaton, and S. G. Louie, Ab initio study of hot carriers in the first picosecond after sunlight absorption in silicon, *Phys. Rev. Lett.* **112**, 257402 (2014).
- [26] J. E. Coulter, E. Manousakis, and A. Gali, Optoelectronic excitations and photovoltaic effect in strongly correlated materials, *Phys. Rev. B* **90**, 165142 (2014).
- [27] J. H. Werner, S. Kolodinski, and H. J. Queisser, Novel optimization principles and efficiency limits for semiconductor solar cells, *Phys. Rev. Lett.* **72**, 3851 (1994).
- [28] R. Brendel, J. H. Werner, and H. J. Queisser, Thermodynamic efficiency limits for semiconductor solar cells with carrier multiplication, *Solar Energy Materials and Solar Cells* **41-42**, 419 (1996).
- [29] W. Spirkl and H. Ries, Luminescence and efficiency of an ideal photovoltaic cell with charge carrier multiplication, *Phys. Rev. B* **52**, 11319 (1995).
- [30] A. D. Vos, Detailed balance limit of the efficiency of tandem solar cells, *Journal of Physics D: Applied Physics* **13**, 839 (1980).
- [31] D. S. Boudreaux, F. Williams, and A. J. Nozik, Hot carrier injection at semiconductor-electrolyte junctions, *Journal of Applied Physics* **51**, 2158 (1980), <https://pubs.aip.org/aip/jap/article-pdf/51/4/2158/18388065/2158>.

